Direct visualization of soliton stripes in the CuO₂ plane and oxygen interstitials in Bi₂(Sr₂₋ₓLaₓ)CuO₆₊δ superconductors

C. Guo,[1] H. F. Tian,[1] H. X. Yang,[1,2] B. Zhang,[1,2] K. Sun,[1,2] X. Sun,[1,2] Y. Y. Peng,[1,2] X. J. Zhou,[1] and J. Q. Li[1,2,3,*]

[1]*Beijing National Laboratory for Condensed Matter Physics, and Institute of Physics, Chinese Academy of Sciences, Beijing 100190, China*
[2]*School of Physical Sciences, University of Chinese Academy of Sciences, Beijing 100049, China*
[3]*Collaborative Innovation Center of Quantum Matter, Beijing 100190, China*

Microstructure features in correlation with the incommensurate modulation and oxygen interstitials in Bi₂(Sr₂₋ₓLaₓ)CuO₆₊δ superconducting materials were studied by Cs-corrected scanning transmission electron microscopy. Atomic displacements following the modulation wave were well characterized by a sinusoidal wave for each atomic layer, which highlighted clear changes resulting from increases in the La concentration. Careful investigations of the alterations in the local atomic structure revealed that remarkable microstructural features, i.e., notable soliton lines, which arise from the prominent interplay between incommensurate modulation and the basic lattice, appear at the CuO₂ sheets yielding visible structural anomalies for x ranging from 0.40 to 0.85. The interstitial oxygen atoms between the SrO-BiO layers became clearly visible for $X \geqslant 0.73$ and showed well-defined ordered states in the $x = 1.10$ sample. These structural features, in particular the strong structural effects of the soliton lines on the CuO₂ sheets, could evidently affect the physical properties of layered La-Bi2201 systems.

I. INTRODUCTION

The Bi₂Sr₂CuO₆ (Bi2201) superconductor is an ideal system to study the physical properties, electronic structure, and mechanism of high-temperature superconductivity [1–7]. It has a simple crystal structure that contains only a single CuO₂ layer in a unit cell, avoiding possible complications from two-layered or multilayered compounds, which may give rise to multiple Fermi surface sheets. Moreover, by replacing Sr²⁺ with some rare-earth ions (R³⁺) combined with an annealing process, one can obtain a wide range of doping levels that span from heavily underdoped, underdoped, optimally doped, to overdoped regions. This is beneficial for investigating the systematic evolution of the electronic structure and physical properties, thus providing clues to understand the physics and mechanism of superconductivity.

Many important insights have been obtained from studying the Bi2201 system. For low-dimensional systems, incommensurate structural modulations, due to their essentially irrational nature with respect to the basic structure, often result in remarkable changes in the crystallographic and physical properties of the systems. For instance, layered Bi₂Sr₂CaₙCuₙ₊₁Oᵧ (BSCCO: $n = 0$, 1, and 2) superconductors contain visible incommensurate modulations yielding large misfits in Bi(Sr) atomic layers [8], and the typical charge density wave (CDW) in TaSe(S)₂ materials shows up in visible discommensuration domains associated with the commensurate-incommensurate phase transition [9]. Theoretical studies have demonstrated that these structural features can be interpreted within the present framework of domain walls, for instance, the CDW discommensuration (i.e., a phase soliton) represents a typical domain wall containing transverse and longitudinal degrees of freedom [10]. Over the last few decades, a variety of investigations have been carried out, especially on the structural features

of the incommensurate modulation in Bi₂Sr₂CaₙCuₙ₊₁Oᵧ ($n = 0$, 1, 2) and on the atomic displacements associated with the modulation in the different layers, as observed by high-resolution transmission electron microscopy (TEM) and x-ray diffraction and analyzed by a few structural models [11].

The structure of the pristine Bi2201 has been studied extensively both by x-ray diffraction (XRD) and transmission electron microscopy (TEM) [12–15]. The basic structure of Bi2201 is an orthorhombic layered structure with cell parameters of $a = 5.362$ Å; $b = 5.374$ Å; $c = 24.622$ Å [12]. An incommensurate superstructure in the b-c plane has been identified by many high-resolution TEM (HRTEM) and electron diffraction studies [15]. Figure S1(a) [16] shows the Cs-corrected scanning transmission electron microscopy (STEM) atomic image of a La-Bi2201 crystal. To better understand the structural modulation, an atomic resolution STEM image of a Bi2212 superconductor is also shown in Fig. S1(b) [16] for comparison for analyzing the structural modulation [16]. This STEM image was taken from thin crystals with a spatial resolution better than 1 Å, according to the method used previously for explaining the atomic structure of layered materials [8]. The relevant structural features and atom positions for the modulations in both Bi2201 and Bi2212 were directly determined. It can be seen that the incommensurate structure in the b-c plane of these superconducting materials can be well characterized by a modulation wave along the b axis, i.e., the wave vectors of $\mathbf{q} = 0.28\mathbf{b}^*$ ($\lambda = 18.6$ Å) for the Bi2201 phase and $\mathbf{q} = 0.22\mathbf{b}^*$ ($\lambda = 24.8$ Å) for the Bi2212 phase as discussed in our previous paper in detail [11]. We herein also show the schematic structures and relevant data as measured from the atomic images in the bottom panel of Fig. S1(c) [16]. These modulations can be briefly written as a sinusoidal wave $\mathbf{D}(r) = \mathbf{A}(\mathbf{b})\sin[2\pi\mathbf{q}\cdot\boldsymbol{r} + \theta(\mathbf{b})] + \mathbf{A}(\mathbf{c})\sin[2\pi\mathbf{q}\cdot\boldsymbol{r} + \theta(\mathbf{c})]$, where $\mathbf{D}(r)$ is the deviation of the atom from the equilibrium position and $\mathbf{A}(\mathbf{b})$ and $\mathbf{A}(\mathbf{c})$ are the amplitude vectors. Careful analysis of the atomic displacements revealed that the $\mathbf{D}(r)$ has clear components

*Corresponding author: ljq@iphy.ac.cn

along the **b** or **c** axis. *r* is the atom position vector, and $\theta(\mathbf{b})$ and $\theta(\mathbf{c})$ are the phases of the modulation. The relevant parameters for structural modulations as obtained from the experimental images are listed in Fig. S1(c) [16]. For Bi2201 and Bi2212 phases, large amplitudes appeared in the CuO_2 layers along the **c** axis. In contrast, the corresponding amplitudes in the **b** direction were very small. In the BiO layers, large atomic shifts associated with structural modulation appeared in the **b** direction, and the amplitude in the **c** direction was very small.

Although the major atomic distortions associated with the structural modulations were extensively investigated in earlier works, the origin of the modulation is not yet completely clear. For instance, Zandbergen *et al.* considered several possible origins for modulations in Bi-superconductors, i.e., (1) extra oxygen atoms in the $(BiO)_2$ layers, (2) structural changes arising from orientation alterations in the lone pairs of Bi ions, and (3) doping effects with several dopants. They concluded that the model with extra oxygen in the $(BiO)_2$ layers demonstrates the best agreement [17]. In our study, careful examinations of the atomic images of the Bi2201 superconductors did not find clear oxygen atoms between the BiO double layers. However, our study of the La-Bi2201 material revealed that interstitial oxygen located between the BiO and SrO layers as discussed in the following context. These experimental data could be useful for understanding the structural properties and superconductivity of Bi-based superconductors. Moreover, in previous investigations, a low-energy electron diffraction study, combined with angle-resolved photoemission (ARPES) analysis, reported a new superstructure ($\mathbf{q_2}$) in the underdoped La-Bi2201 samples [1,4,11]. Our TEM observations demonstrated that this $\mathbf{q_2}$ possibly arises from changes in the stacking behavior of the conventional modulation ($\mathbf{q}$). In fact, the $\mathbf{q_2}$ modulation was visible only in the [001] zone-axis diffraction pattern coexisting with the $\mathbf{q}$ modulation [11], which can be interpreted by an antiphase stacking of the $\mathbf{q}$ modulation and visible influence from the diffraction spots at the high-order Laue zones. Considering the layered structural features and strong structural modulation along the *b* axis, our structural investigations revealed that a clearer and better view of the incommensurate modulation, atomic displacements, and soliton stripes/domains could be obtained from samples oriented with the [100] axis parallel to the incident electron beam. Moreover, multiple reflections from the high-order Laue zones are no longer a problem in this case because the lattice parameter of the *a* axis (5.4 Å) is much smaller than that of the *c* axis (25 Å). Furthermore, the stacking faults along the *c* axis, as a common defective structure in the present system, are now viewed edge-on and can be avoided completely by choosing an area free of stacking faults.

In the present study, our observations demonstrated that the structural modulation in the CuO_2 layers is relatively stronger in the presence of Bi2201 compared to that in the presence of Bi2212 superconductor. Moreover, careful investigations of local structural alterations revealed certain novel features in the $Bi_2Sr_{2-x}La_xCuO_{6+\delta}$ materials: (1) notable soliton lines appear at the CuO_2 sheets with remarkable structural anomalies in the samples with $0.40 \leqslant x \leqslant 0.85$ and (2) interstitial oxygen atoms between the SrO-BiO layers adopt well-defined ordered states in the $x = 1.10$ sample. It is believed that these structural features, in particular the strong structural effects of the soliton lines on the superconducting CuO_2 sheets, could evidently affect the physical properties of layered Bi-superconducting materials.

II. EXPERIMENT

The polycrystalline parent phase of $Bi_2Sr_2CuO_{6+\delta}$ (Bi2201) was synthesized by a conventional solid-state reaction method. All the La-doped $Bi_2(Sr_{2-x}La_x)CuO_{6+\delta}$ (La-Bi2201) single crystalline samples used in our TEM studies were grown by the traveling solvent floating zone technique [18]. Post-annealing procedures were performed to obtain compositionally uniform crystals. Structural characterizations and the chemical compositions of the crystals were measured by XRD and induction-coupled plasma atomic emission spectroscopy, respectively. The actual compositions were very close to their nominal compositions. Resistivity, magnetic susceptibility, and the details of sample synthesis and characterization were reported in a previous paper [18].

Cross-sectional TEM specimens were prepared using a focused ion beam system and also by mechanical polishing followed by ion milling at liquid nitrogen temperature, while plane-view specimens were cleaved using adhesive tape and then dissolved in a chloroform solution and deposited on a carbon film suspended on a copper grid. The thickness of samples was less than 30 nm. High angle annular dark field (HAADF) and annular bright field (ABF) STEM images were performed on JEOL ARM200F TEM equipped with probe-forming spherical-aberration corrector. The electron dose rate is 0.4 pA/cm^2. The semiconvergence angle is about 23 mrad. The inner and outer angles of the detectors are 90 and 370 mrad for HAADF images, and 11 and 22 mrad for ABF images, respectively. The ABF-STEM image was simulated using the multislice algorithm via the QSTEM software. The spherical aberration coefficient was set to 1 μm. The defocus and thickness used in the STEM images were 2 and 6.8 nm, respectively.

III. RESULTS AND DISCUSSION

In fact, based on an extensively high-spatial-resolution STEM investigation, there are two important structural phenomena in $Bi_2Sr_{2-x}La_xCuO_{6+\delta}$ with *x* ranging from 0.40 to 1.10: (a) anomalous atomic displacements occur in CuO_2, which can be understood as the excitations of soliton strips and (b) oxygen interstitials can be clearly seen in the samples with La content from 0.85 to 1.10. Figure S2 [16] in the Supplemental Material shows a phase diagram of $Bi_2(Sr_{2-x}La_x)CuO_{6+\delta}$ [16] and certain novel structural features observed in the present study [19].

In the La-Bi2201 samples, we observed a type of structural anomaly, which can be well explained by the appearance of soliton stripes. Indeed, the phase solitons as elementary excitations have been extensively investigated for one-dimensional (1D) incommensurate phases [10,20]. Figure 1 shows a micrograph of the atomic structure of $Bi_2Sr_{2-x}La_xCuO_{6+\delta}$ with $x = 0.40$ and the relevant analysis on atomic displacements as seen along the [100] zone axis. The notable structural distortions associated with the structural modulation in all atomic layers are well demonstrated. Moreover, the most striking structural
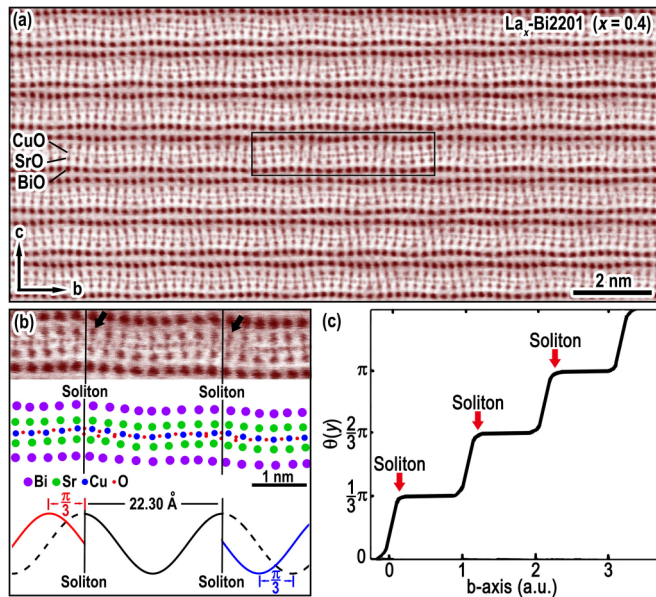
FIG. 1. (a) High-spatial-resolution ABF STEM image of $Bi_2(Sr_{2-x}La_x)CuO_{6+\delta}$ with $x = 0.40$. (b) Highly magnified atomic resolution image and schematic diagram showing the appearance of phase slip on the soliton line. (c) Schematic diagram explaining the phase soliton in the CuO_2 sheets of the $x = 0.40$ sample.

anomalies as indicated by arrows in Fig. 1(b) appear evidently in the CuO_2 layers, which yield visible lattice mismatches in the CuO_2 layers arranged periodically along the b axis. These defective structures apparently break the periodic array of the modulation wave.

In past decades, excitations of soliton lines and the relevant structural domains as significant issues have been extensively discussed in various low-dimensional materials. For instance, discommensurations have been well analyzed within the framework of Landau theory [21,22] as the typical type of soliton lines in CDW systems and observed experimentally following structural transformations from the commensurate to incommensurate phase [9,23]. It has also been demonstrated that the evolution and nucleation of soliton stripes clearly correlate with the changes in the translational symmetry and the defective structures [10,21,22,24]. It has also been verified that the formation of soliton stripes can result in notable structural and physical properties of modulated systems [25].

In CDW materials, the dark-field TEM images using satellite spots can reveal the CDW domains, discommensurations (i.e., the phase soliton), and their structural evolutions. This technique in general shows a spatial resolution of hundreds of nanometers in the experimental images. However, our structural investigations of the $Bi_2Sr_{2-x}La_xCuO_{6+\delta}$ materials clearly revealed that the soliton stripes appear on a spatial scale as small as a few nanometers; therefore, in the present study, the high-resolution STEM images were first used for characterizing the atomic displacements associated with structural modulation and soliton domains, as clearly illustrated in Fig. 1(a) for the $x = 0.40$ superconductor.

Figure 1(b) shows an ABF-STEM image at a higher magnification clearly exhibiting the atomic structural features of the $x = 0.40$ sample. In addition to the structural modulation in all

atomic layers as discussed in the above context, we can clearly observe the remarkable atomic misfits appearing at the CuO_2 layer. This remarkable structural feature can be quantitatively understood by the soliton stripes excited in the CuO_2 sheets as proposed theoretically for the incommensurate phase [9,22]. Moreover, the lattice mismatches are often shown a width over a few lattice planes within the CuO_2 sheets. This fact clearly suggests that the soliton lines do not proceed straight along the view direction but adopt a winding way through the superconducting crystals. This feature is also discussed for the $x = 0.85$ sample. It can clearly be seen that this type of structural anomaly breaks the translational symmetry of a crystal lattice at the superconducting CuO_2 sheets; therefore, it can also affect the relevant physical properties of the present system. In sharp contrast with what was observed in the CuO_2 layers, the other atomic layers (the BiO and SrO layers) showed a clear structural modulation, but no anomalous structural features were observed. It is known that La doping introduces electron carriers into the CuO_2 sheets, so it is highly likely that the appearance of soliton stripes arises fundamentally from the strong electron correlation and electron-lattice interactions in this layered superconductor. In the phase diagram shown in Fig. S2 [16], we can see that the soliton domains arise in the CuO_2 sheets with $0.40 \leqslant x \leqslant 0.85$ in $Bi_2(Sr_{2-x}La_x)CuO_{6+\delta}$, with the decrease in T_c, which reveals the correlation between T_c and the continuity of the CuO_2 sheets [16].

Theoretical investigations on local atomic displacements at the soliton line have also been discussed in a previous study [23]. In particular, the phase slip on a soliton line was studied by McMillan for 1D incommensurate modulation and conformed experimentally in the CDW phase $2H$-$TaSe_2$ [10,21,22]. In the present study, we performed our analysis following the reported method for the experimental images. A notable phase slip appeared on the soliton line as schematically illustrated in Figs. 1(b) and 1(c). The modulation wave in general has a phase slip of $\pi/3$, which can be directly measured from the high-resolution STEM images as indicated in Fig. 1(b). However, it is suggested that the average spacing (L) of the soliton stripe can be estimated from the measurements of incommensurability (δ_i) in the modulation wave using $L = 2\pi/3\delta_i$. Our calculation demonstrated that the experimental data ($L_{expt} = 1.7$ nm) in many areas are comparable with the theoretical data ($L_{Theor} = 2$ nm) [10].

On the basis of the fundamental theoretical results reported by McMillian [10,21,22] and our experimental observations, the phase slip on the soliton line in the La-Bi2201 superconductors can be written as follows: $\theta(y) = \theta(y) + 2m\pi/6$, where m is an integer and y is the position of the soliton lines along the modulation direction (i.e., the b axis). Figure 1(c) shows the data illustrating phase slips upon the appearance of soliton stripes, which highlights similar features as discussed in Ref. [10]. The phase slip on the boundary is $\Delta\theta = \pi/3$. Figure 1(b) shows the experimental image, local atomic displacements, and schematic phase slips on the soliton line, in which a good agreement between experimental and theoretical data is evidenced.

The local structural features and arrangement of the soliton domains appear to be dependent on the La concentration and local strains in the La-Bi2201 samples. In fact, we examined the microstructure and structural modulation features of all
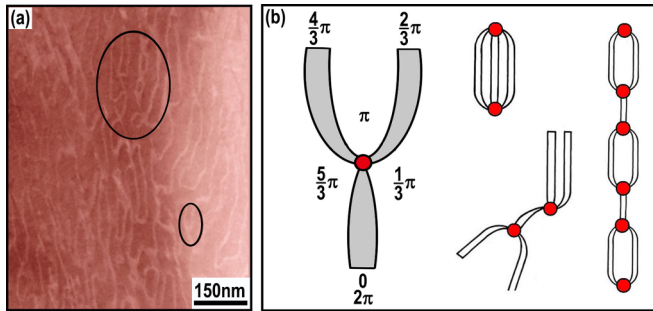
FIG. 2. (a) Dark-field TEM image showing the configurations of the stripe lines in some regions. (b) Schematic line diagrams illustrating the configurations of the soliton domain patterns observed in our experimental investigations.

FIG. 3. (a) High-spatial-resolution ABF STEM image of $Bi_2(Sr_{2-x}La_x)CuO_{6+\delta}$ with $x = 1.10$, revealing that the interstitial oxygen appears between the SrO and BiO layers. (b) Highly magnified image of the area in (a). (c) A simulated ABF STEM image. (d) A superstructure model based on the experimental images.

the samples with $0 \leqslant x \leqslant 1.10$. It was found that the soliton domain occurs if the La doping increases and the carrier concentration rises to $p = 0.15$ ($x = 0.40$) as estimated in Ref. [19], and the distribution of the soliton line and its density often demonstrated remarkable alterations. In certain regions, the density was high with clear lattice misfits as shown in Fig. 1(a). A crystal with a low density in the soliton line and lattice misfits was also visible as shown in Fig. S3 [16]. It is known that the formation of the soliton line is favored when there is competition between the terms in the Landau free energy arising from the overlap of the multiperiodic modulations [22,24], i.e., an essential commensurability force arises from the strong coupling between the modulation wave and the basic perovskite sublattice in the Bi-based superconductors; therefore, this long modulation wave demonstrates both transverse and longitudinal components.

To reveal the structural features and the pathway of the soliton line running through the Bi2201 crystals, and in particular the vortex pattern of the soliton domains [10], we slightly tilted the sample off the [100] direction. From the dark-field TEM images, we can clearly see the configuration of the stripe lines in certain regions, as shown in Fig. 2(a) for $x = 0.85$. A similar technique was also used in high-resolution structural observations of the soliton lines in Ag-Mg alloys [26]. For the purpose of discussion and arguments, let us assume that the alteration in the image contrast for stripes essentially arises from the phase slip across a soliton line, which could yield different diffraction effects between neighboring domains for electron imaging as shown in Fig. 2(a). Additionally, we have performed high resolution ABF-STEM observations for soliton stripes as typically shown in the Fig. S4 in the Supplemental Material [16]. In Fig. 2(b) we illustrate clearly the phase relationship of the domains around a vortex center, where each boundary yields a phase slip of $\pi/3$. Figure 2(b) also shows a schematic of the line diagrams illustrating a few configurations of the soliton domain patterns as observed in our experimental investigations.

Furthermore, it is an important issue in the high-T_c superconductors that the physical properties and local structural features evidently depend on the oxygen interstitials. Previous structural studies on the Bi2212 phase have suggested that oxygen interstitials between the double Bi-O layers could result in structural modulation and changes in carrier density
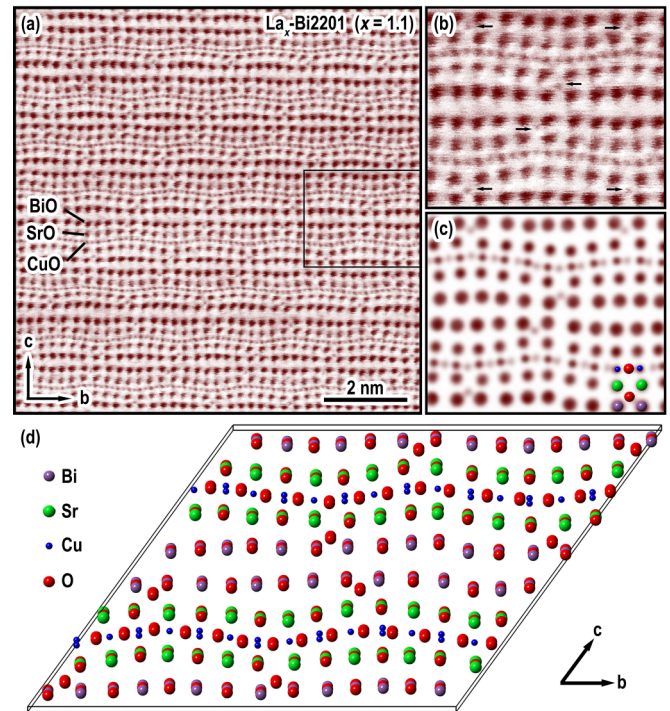
for the superconductivity [8]. In view of the sensitivity of sample characteristics to sample preparation conditions, our studies on the oxygen interstitials (ordering) have been conducted on samples that are fully characterized and have known physical properties from previous studies [1,9]. As revealed by the Cs-corrected ABF-STEM observations, the interstitial oxygen in La-Bi2201 crystals actually appears between the SrO and BiO layers and are local in the center of the Sr-Sr-Bi-Bi tetrahedrons as shown in Figs. 3(a) and 3(b) for the $x = 1.10$ sample. The black dots can be interpreted as columns of Bi, Sr(La), Cu, and O atoms projected along the [100] zone axis. To confirm the interstitial atoms are oxygen, the corresponding HAADF image of Fig. 3(a) has been shown in the Fig. S5 in the Supplemental Material [16]. As expected, the oxygen interstitials and O atoms of CuO layers are invisible in the HAADF image. The oxygen interstitial periodic is part of the structure modulation for $x = 1.10$. It will significantly alter the valence state of other cations and affect the superconductivity. The ABF-STEM simulation and superlattice structural model are shown in Figs. 3(c) and 3(d). Moreover, a pseudocolor image of Fig. 3(a) has also been shown in Fig. S5(b) of the Supplemental Material [16]. Interestingly, the intensity of Sr atoms are periodic in the SrO layers, which indicates that the substitution rate may be modulated. Although the appearance of oxygen interstitials can be observed in all the $x \geqslant 0.73$ samples, the ordered behavior and occupation clearly depends on the La concentrations. The samples with $x = 0.73$ and 0.85 show notably random intestinal atoms, and for the $x = 0.73$ sample, the ordering appears only in the range

TABLE I. Interstitial value (δ) of oxygen, the maximum interstitial value (δ_{max}), and the interstitial oxygen occupancy (β) for different La concentrations x in La-Bi2201.

x	δ	δ_{max}	β
0.40	0.20	0.47	0.43
0.73	0.37	0.48	0.77
0.85	0.43	0.50	0.86
1.10	0.55	0.57	0.96

as short as 5 nm, and clearly ordered states were observed in the $x = 1.10$ sample. From the experimental images, we constructed a superstructure model as shown in Fig. 3(d). This oxygen ordering is found to be strongly coupled with structural modulation along the [010] direction. In the structural model and STEM images, a well-defined ordered state appearing in a range larger than 100 nm can be clearly observed. If the interstitial ordering is assumed to be homogeneous in the sample, this type of oxygen ordering can be characterized by a wave vector of $\mathbf{q} = 0.28\mathbf{b}^*$, which is in agreement with the experimental data of the $x = 1.10$ sample.

Indeed, based on the experimental observations, we also made an attempt to estimate the excess oxygen content by analyzing the changes in contrast of the atomic images. However, La substitution for Sr atoms can introduce electrons into the CuO_2 sheet to adjust and control the superconductivity, and the appearance of oxygen interstitials will give rise to another issue that affects charge carriers and local structural features. In Table I we just show a brief estimation and discussion based on the structural and chemical analyses. Considering the La^{3+} substitution for Sr^{2+}, δ is the interstitial value of oxygen for maintaining a valence balance in $Bi_2(Sr_{2-x}La_x)CuO_{6+\delta}$, and δ_{max} is the maximum value of the interstitials in our structural model. β is the interstitial oxygen occupancy as estimated from the STEM image contrast. It is worth noting that the interstitial oxygen occupancy showed a clear rising tendency with the increase in the La content, and the well-defined ordered state was observed only in the La-Bi2201 ($x = 1.10$) sample. In fact, the formation of this interstitial ordered state in the present system can also be understood as a structural phase transition at around $x = 0.85$, which is driven by the oxygen ordering. This structural phase transition allows the La-Bi2201 materials to become non-superconductors at around $x = 0.85$ as discussed by the phase diagram of superconductivity [19].

IV. CONCLUSIONS

In summary, we performed an extensive investigation of the microstructural features in correlation with the incommensurate modulation and the oxygen interstitial in $Bi_2(Sr_{2-x}La_x)CuO_{6+\delta}$ superconducting systems by Cs-corrected STEM. As observed in the high-resolution STEM images, the atomic displacements in each atomic sheet were characterized by a sinusoidal wave model and discussed in comparison to the Bi2212 superconductor. Importantly, our structural study clearly revealed the presence of soliton domains in the CuO_2 sheets in $Bi_2(Sr_{2-x}La_x)CuO_{6+\delta}$ with $0.40 \leqslant x \leqslant 0.85$, and the phase slip at the soliton domain wall was found to be $\pi/3$ from the high-resolution STEM images. This structural phenomenon essentially arises from the interplay between incommensurate modulation and the basic lattice, which can result in remarkable changes in modulation waves. The strong structural effects of the soliton lines on the superconducting CuO_2 sheets could evidently affect the superconductivity. Moreover, the oxygen interstitials and relevant ordered state were also investigated and discussed in correlation with the alteration of the microstructural features in these layered superconducting materials. The periodic oxygen interstitials in many areas are found to be associated with the structure modulation, which could significantly alter the valence state of other cations and affect the physical properties of Bi-superconducting materials.

[1] J. Meng, G. Liu, W. Zhang, L. Zhao, H. Liu, X. Jia, D. Mu, S. Liu, X. Dong, J. Zhang, W. Lu, G. Wang, Y. Zhou, Y. Zhu, X. Wang, Z. Xu, C. Chen, and X. J. Zhou, Nature (London) **462**, 335 (2009).

[2] M. Hashimoto, R.-H. He, K. Tanaka, J.-P. Testaud, W. Meevasana, R. G. Moore, D. Lu, H. Yao, Y. Yoshida, H. Eisaki, T. P. Devereaux, Z. Hussain, and Z.-X. Shen, Nat. Phys. **6**, 414 (2010).

[3] I. Zeljkovic, E. J. Main, T. L. Williams, M. C. Boyer, K. Chatterjee, W. D. Wise, Y. Yin, M. Zech, A. Pivonka, T. Kondo, T. Takeuchi, H. Ikuta, J. Wen, Z. Xu, G. D. Gu, E. W. Hudson, and J. E. Hoffman, Nat. Mater. **11**, 585 (2012).

[4] R. H. He, M. Hashimoto, H. Karapetyan, J. D. Koralek, J. P. Hinton, J. P. Testaud, V. Nathan, Y. Yoshida, H. Yao, K. Tanaka, W. Meevasana, R. G. Moore, D. H. Lu, S.-K. Mo, M. Ishikado, H. Eisaki, Z. Hussain, T. P. Devereaux, S. A. Kivelson, J. Orenstein, A. Kapitulnik, and Z.-X. Shen, Science **331**, 1579 (2011).

[5] A. Sugimoto, S. Kashiwaya, H. Eisaki, H. Kashiwaya, H. Tsuchiura, Y. Tanaka, K. Fujita, and S. Uchida, Phys. Rev. B **74**, 094503 (2006).

[6] M. C. Boyer, W. D. Wise, K. Chatterjee, M. Yi, T. Kondo, T. Takeuchi, H. Ikuta, and E. W. Hudson, Nat. Phys. **3**, 802 (2007).

[7] W. D. Wise, M. C. Boyer, K. Chatterjee, T. Kondo, T. Takeuchi, H. Ikuta, Y. Wang, and E. W. Hudson, Nat. Phys. **4**, 696 (2008).

[8] Y. Gao, P. Lee, P. Coppens, M. A. Subramanian, and A. W. Sleight, Science **241**, 954 (1988).

[9] T. Ishiguro and H. Sato, Phys. Rev. B **52**, 759 (1995).

[10] W. L. McMillan, Phys. Rev. B **14**, 1496 (1976).

[11] Z. Chen, Y. Peng, Z. Wang, Y. J. Song, J. Meng, X. J. Zhou, and J. Q. Li, Supercond. Sci. Technol. **26**, 055010 (2013).

[12] C. C. Torardi, M. A. Subramanian, J. C. Calabrese, J. Gopalakrishnan, E. M. McCarron, K. J. Morrissey, T. R. Askew, R. B. Flippen, U. Chowdhry, and A. W. Sleight, Phys. Rev. B **38**, 225 (1988).

[13] J. G. Wen, Y. Liu, Z. F. Ren, Y. F. Yan, Y. Q. Zhou, and K. K. Fung, Appl. Phys. Lett. **55**, 2775 (1989).

[14] M. Yoshio, T. Shunji, H. Shigeo, and U. Akihiro, Jpn. J. Appl. Phys. **27**, L1873 (1988).

[15] J. Q. Li, C. Chen, D. Y. Yang, F. H. Li, Y. S. Yao, Z. Y. Ran, W. K. Wang, and Z. X. Zhao, Z. Phys. B **74**, 165 (1989).

[16] See Supplemental Material at http://link.aps.org/supplemental/ 10.1103/PhysRevMaterials.1.064802 for further information on experimental details.

[17] H. W. Zandbergen, W. A. Groen, F. C. Mijlhoff, G. V. Tendeloo, and S. Amelinckx, Physica C **156**, 325 (1988).

[18] J. Meng, G. Liu, W. Zhang, Z. Lin, H. Liu, L. Wei, X. Dong, and X. J. Zhou, Supercond. Sci. Technol. **22**, 045010 (2009).

[19] J. B. Peng and C. T. Lin, J. Supercond. Nov. Magn. **23**, 591 (2010).

[20] W. P. Su, J. R. Schrieffer, and A. J. Heeger, Phys. Rev. B **22**, 2099 (1980).

[21] W. L. McMillan, Phys. Rev. B **12**, 1187 (1975).

[22] W. L. McMillan, Phys. Rev. B **12**, 1197 (1975).

[23] C. H. Chen, J. M. Gibson, and R. M. Fleming, Phys. Rev. B **26**, 184 (1982).

[24] P. Bak and V. J. Emery, Phys. Rev. Lett. **36**, 978 (1976).

[25] I. B. Goldberg, H. R. Crowe, P. R. Newman, A. J. Heeger, and A. G. Macdiarmid, J. Chem. Phys. **70**, 1132 (1979).

[26] Y. Fujino, H. Sato, M. Hirabayashi, E. Aoyagi, and Y. Koyama, Phys. Rev. Lett. **58**, 1012 (1987).